3. Overview on the North Anatolian Fault Zone (NAFZ)

The North Anatolian Fault Zone (NAFZ) is an active right-lateral system, about 1500 km long, which bounds to the north the Anatolian block. It represents a transform margin that mainly follows a pre-existing zone of crustal weakness: a suture zone inherited from an earlier collisional phase [Sengör and Yılmaz, 1981; Şengör et al., 1985; Okay, 1989; Yılmaz and Yılmaz, 2004].

In the following, we synthesize the tectonic setting of the area through three points: the general tectonic setting ; the onset, growth and present-day setting of the NAFZ; the study area.

3.1. General tectonic setting

The Anatolian area underwent a series of multiple continental collisions and, probably starting from Carboniferous, was comprising the site of oceans subsequently closed. Thus, the history of sedimentation, deformation, ophiolite emplacement and metamorphism is complicated. Since the Mesozoic, a N-S convergence along the Alpine-Himalayan system, which includes also Turkey, the Aegean Sea and Greece, was active and many oceanic floors have been abducted between different continental lithospheres [*e.g.*, Ketin, 1966; Aubouin and Dercourt, 1970; Şengör 1979; Barka, 1981; Şengör and Yılmaz, 1981].

In Turkey mainland, remnants of the oceanic materials (ophiolites) are visible as continuous suture zones between continental fragments, that are part of imbricate structures approximately EW trending [*e.g.*, Sengör and Yılmaz, 1981; Jackson and McKenzie, 1988; Görür et al., 2000] (fig. 3.1.1.). Three principal suture zones are present in Turkey: The Intra-Pontide, to the north [*e.g.*, Sengör et al., 1985; Okay, 1989]; the Izmir–Ankara–Erzincan [Şengör 1979; Stampfli and Mosar., 1998; Robertson et al., 2004]; the Antalya (Lycian) suture zone and the SE Turkish (Bitlis-Zagros) suture [*e.g.*, Mueller & Kahle, 1993].

In northwest Turkey, The Intra-Pontide suture zone forms the boundary between two domains: the southern Istanbul zone (or western Pontidi) and the northern Sakarya zone. The Izmir–

Ankara–Erzincan suture forms the boundary between two former continental fragments, the Sakarya Zone in the north and the Anatolide–Tauride Block in the south [Sengör and Yılmaz, 1981; Okay and Tüysüz, 1999].

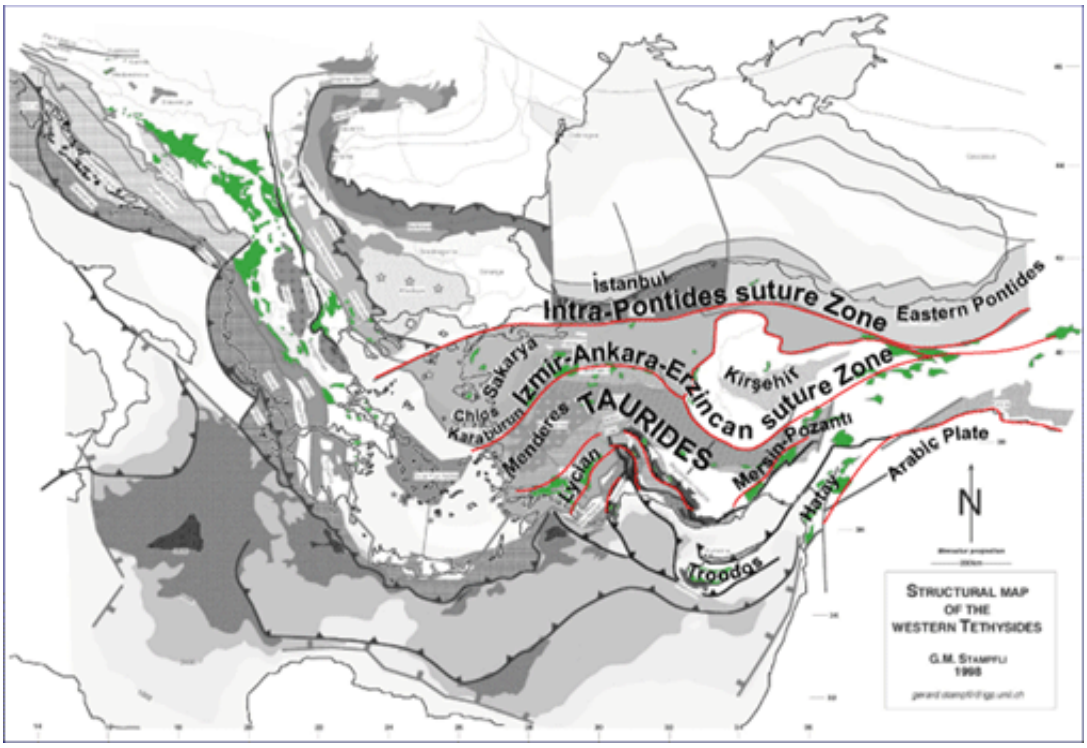

Figure 3.1.1. Outline tectonic map showing the main sutures in the Eastern Mediterranean orogen (from Stamfli et al. [1998]).

According to some Authors [Sengör and Yılmaz, 1981; Sengör et al., 1985; Yılmaz, 1989; Yılmaz, 1990], the compressional orogenic regime, in the Anatolian block, continued until the Early Miocene. The collisional zone migrated southwestward or southward from Cretaceous, down to the present position of the Cyprus-Hellenic subduction zone [Sengör et al., 2003, and reference therein].

In the eastern Anatolia, more than 30 Ma, the shortening between Arabia and Eurasia started and the Arabic plate collided with Eurasia along the Bitlis-Zagros suture [Aktas and Robertson, 1984; Michard et al. 1984; Hempton, 1985]. As a result of the contraction, the Anatolide–Tauride Block, which was below sea level until the middle Miocene, underwent a strong uplift during the successive phases, up to 1000 m relative to the central Anatolian plate. [Sengör et al., 1985; [Barka and Reilinger, 1997; Emre et al., 1998; Brun et al., 2005]. The average crustal thickness of the

overthickened crust resulting from the post-Eocene N-S intracontinental shortening, is estimated to have been 50-60 km in central Anatolia, 30-45 km in western Anatolia [Rodgers et al., 1997; Zor et al., 2003]. While collision was initiating to the east, extension was already taking place to the west, in the Aegean and northwestern Anatolian zones [Angelier et al., 1982; Mercier et al., 1989; Seyitoglu et al., 1992; Jolivet et al., 1994].

3.2. The North Anatolian Fault Zone

3.2.1. Onset and growth of the NAF

Deformations affecting the Anatolian-Aegean regions provide evidence for stress regime changes occurring during the Neogene: the onset of the strike-slip regime, and the development of the East Anatolian Fault (EAF) and NAFZ (fig. 3.2.1). Between Upper Miocene and early Pliocene, in the East Anatolian plateau and Lesser Caucasus a drastic change from NNW-trending compression to strike-slip faulting has been recognized [Kocygit et al., 2001; Ozden et al., 2002]. Also the volcanic complexes testify this change of the stress regime. In fact, two main magmatic signatures occur in Anatolia area since Miocene times: 1) typical subduction-related, southwestward migrating Miocene to Present calk-alcaline volcanism and 2) Upper Miocene-Quaternary alkaline Na-rich magmatism [Benda et al., 1974; Yılmaz et al., 2001].

The EAF (fig. 3.2.1) became active around 15Ma, for a length of ca. 600 km, with a nearly straight fault trace trending NE–SW, from the Dead Sea Fault to the North Anatolian Fault [McKenzie 1972 and 1976; Muehlberger and Gordon 1987]. The East Anatolian Fault has accommodated mostly left-lateral slip [Westaway and Arger 1996; McClusky et al. 2000; Khale et al. 2000] and crosscuts, folded structures related to the beginning of the Arabia-Eurasia collision [Westaway and Arger 1996].

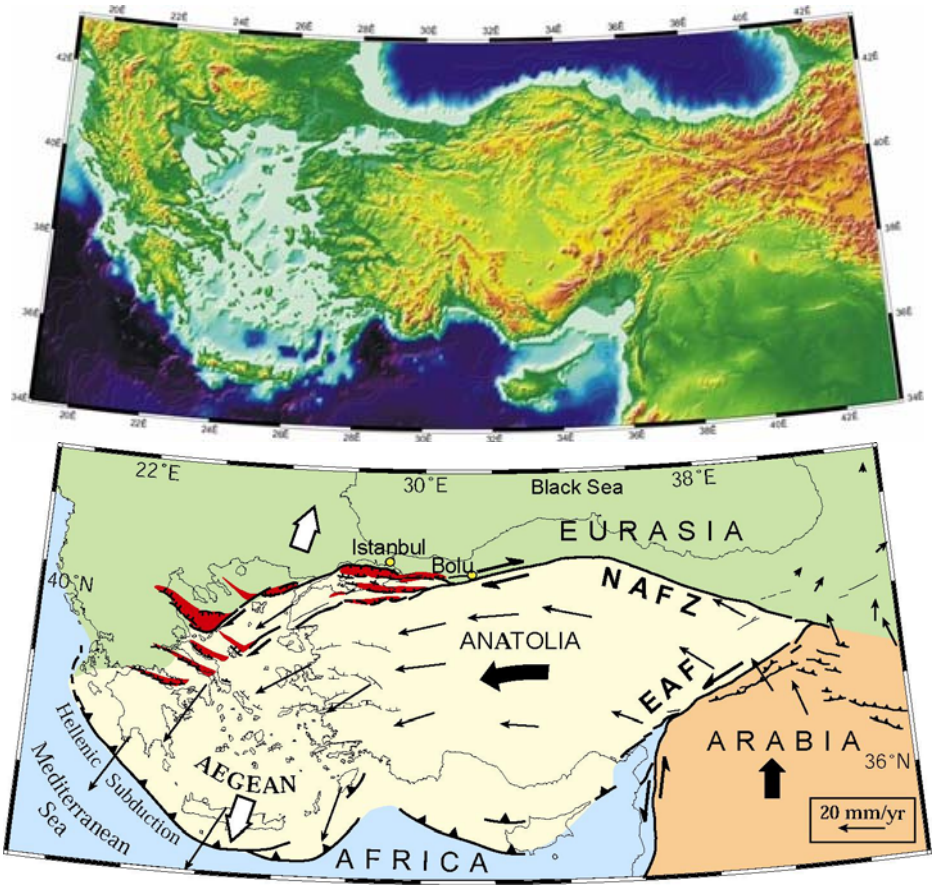

Figure 3.2.1. Top) Shaded relief of eastern Mediterranean. Bottom) Tectonic setting of eastern Mediterranean. Anatolia-Aegean block moves westward, toward Hellenic subduction zone. Current motion relative to Eurasia (GPS [Global Positioning System] and SLR [Satellite Laser Ranging] velocity vectors, in mm/yr [Reilinger et al., 1997]). In Aegean a localized, fast transtension (red areas) is associated with later, westward propagation of North Anatolian fault (NAFZ). (modified from Armijo et al. [1999]).

The timing of the NAF formation is controversial. Based on the age of fault-related basins deposits, The NAFZ is supposed to be active since Late Miocene [Şengör et al., 1985; Dewey et al., 1986; Şengör et al., 2005] (fig. 3.2.2), starting from its easternmost part, the triple junction with the EAF [Şengör et al. 1985].

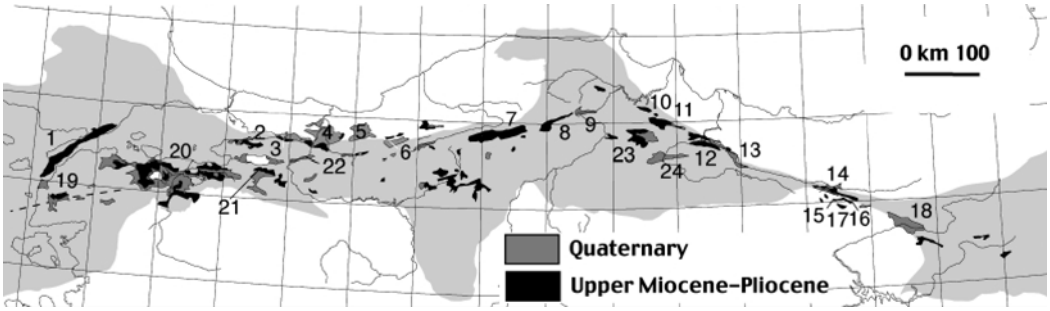

Figure 3.2.2. Fault-related basin along the North Anatolian Shear Zone. (from Şengör et al. [2005]).

Conversely, based on the analysis of mesoscopic structures Barka and Hancock [1984] and Barka [1985] suggested that the fault zone might have been initiated as a wide shear zone, probably during the end of Late Miocene, and they interpreted the angular unconformity of the near-fault basin infill as the Early Pliocene fault onset (fig. 3.2.3.).

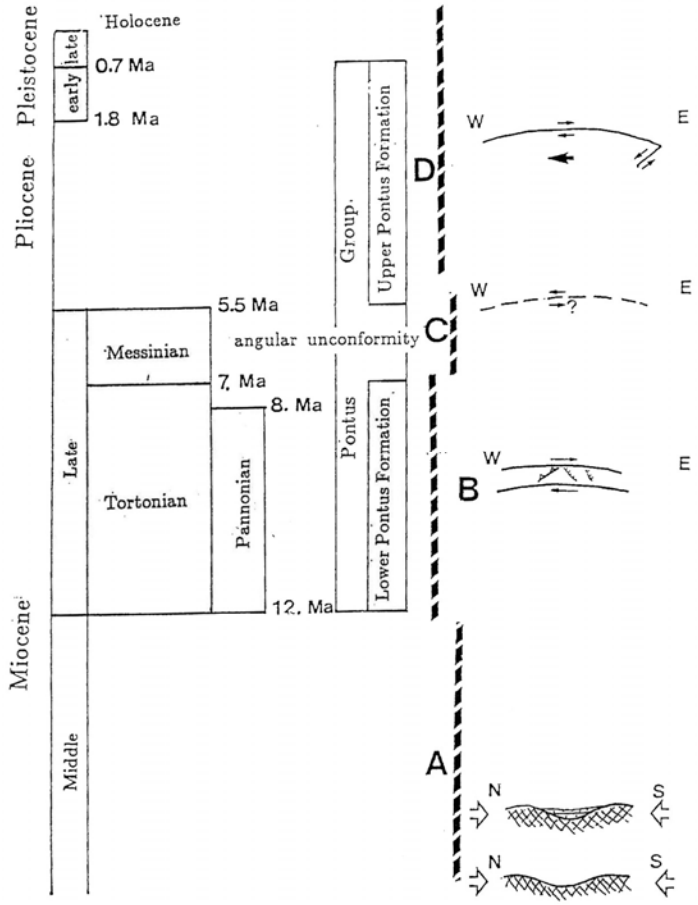

Figure 3.2.3. Tectonic stages of Anatolia since the beginning of the middle Miocene. Stage A: N-S compression, as a result of which compressional basins were formed. Later, the sediment of these basins were compressionally deformed. Stage B: initial formation of the North Anatolian Fault as a wide shear zone. Stage C: Messinian. Stage D: Formation of the North Anatolian Fault as a narrow shear zone. (from Barka [1985]).

Many Authors agree on a westward time-space propagation of the NAF to Central Anatolia (Early Pliocene), to the Marmara region (early to Middle Pliocene), then to the Aegean Sea (late Pliocene) (fig. 3.2.4). In the central part, the age of initiation of the NAF can be constrained to the early Pliocene by lacustrine sediments filling pull-apart basins [Andrieux et al., 1995]. On the basis of geological observations, Hubert-Ferrari et al. [2002] argue that the base of the sedimentary pile

should be older than 5 Ma, but younger than the 8.5 Ma volcanic series over which it lies. Dhont et al. [1998] suggests that the present-day strike-slip NAF, within its central part, did not exist before early Pliocene, agreeing with the Miocene-Pliocene onset [Andrieux et al., 1995; Over et al., 1997; Bellier et al., 1997]. The change in orientation of the strike-slip segments of the NAFS has been also explained by the eastward propagation of the fault: the N100° oriented eastern segment of the NAF, initiated before the western N75° segment [*e.g.*, Şengör, 1979; Yaltirak et al., 2000].To the West, in the Marmara region, the arrival of the NAF is bracketed between 5 [Kocyigit et al., 2001] and 3.5 Ma [Le Pichon and Angelier, 1979; Agard et al., 2005; Şengör et al. ,2005]. On the northern Aegean trough (5 in fig. 3.2.4), prosecution of the NAF is accommodated by more distributed deformation with N110° extensional structures and N40° dextral main faults thought to have propagated in the late Pliocene.

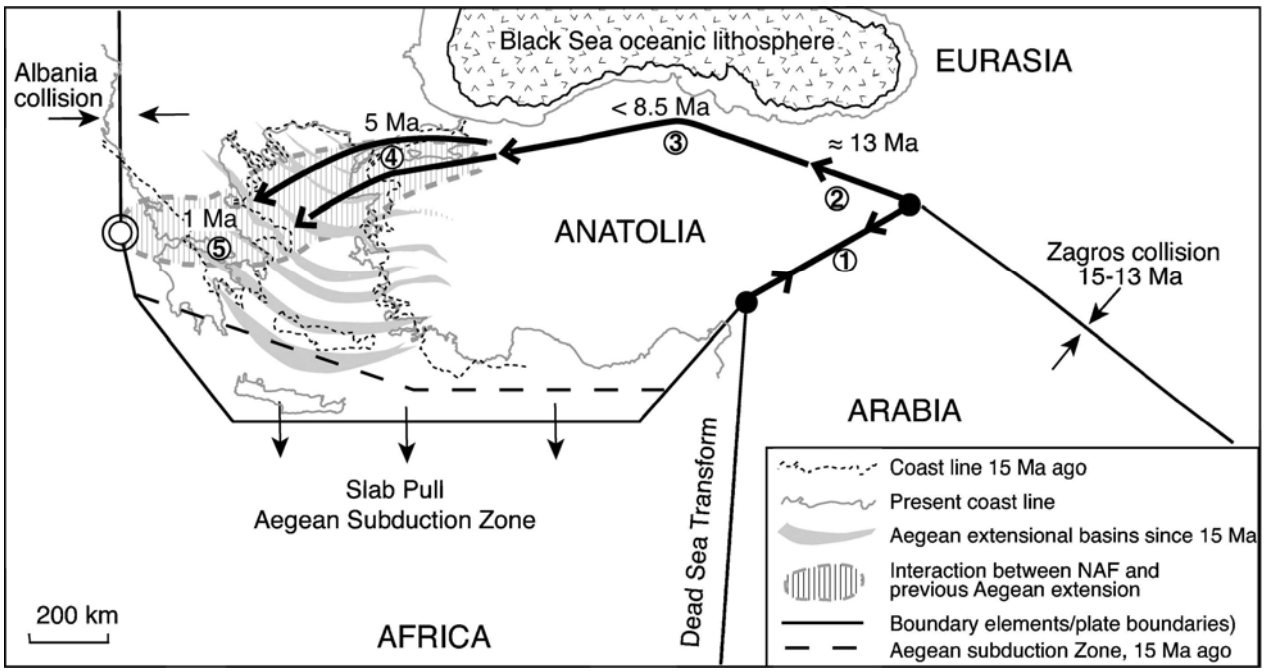

Figure 3.2.4. Propagation of the North Anatolian Fault (NAF). Initiated in the east during the uplift of the Anatolian Plateau and after the formation of the East Anatolian Fault (1, 2). The NAF propagated across north Anatolia (3) and reached the Marmara Sea 5 Ma ago (4) and the Gulf of Corinth 1 Ma ago (5). When the NAF entered the Aegean region, it interacted with the existing active extensional structures. Black lines represent present plate-boundary geometry. (from Hubert-Ferrari et al. [2003]).

Conversely, Şengör et al. [2005] consider the NAF as a diachronous structure that formed by progressive strain localization into a coeval, westerly widening, shear zone (NASZ) (fig. 3.2.5), that has formed since approximately 11 Ma ago. Inside this shear zone, only the NAF, the localized principal deformation zone, is supposed to have a diachronous evolution and may have propagated westward at an average rate of 11 cm/year. The NAF reached the Sea of Marmara no earlier than 200 ka ago, although the NASZ-related deformation there commenced in the Late Miocene.

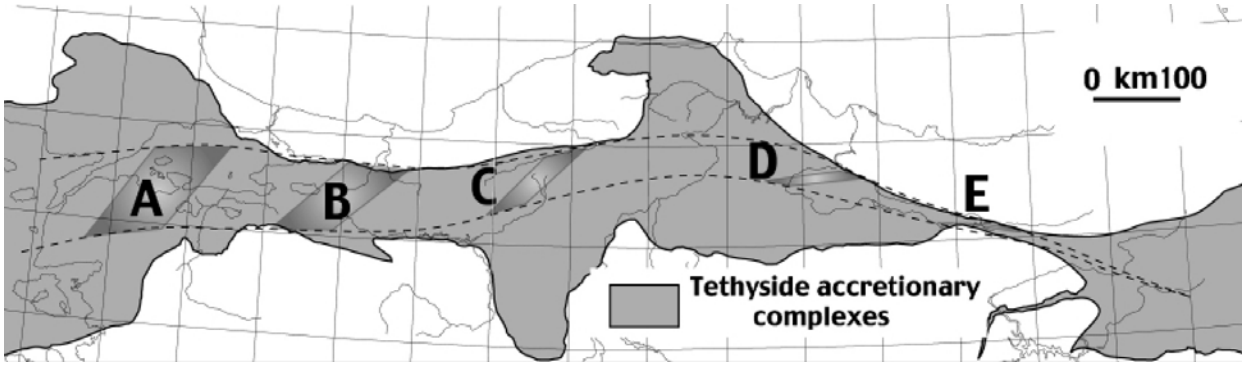

Figure 3.2.5. Theoretical structural evolution of the North Anatolian Shear Zone (NASZ, zone between dashed lines) ends up in the localization of the deformation on a single active strand: the North Anatolian Fault (NAF). The five quadrilaterals (A, B, C, D, E) are used to show the variation in shear strain distribution along the NASZ: distributed deformation to the west, with a young northern active NAF and localized deformation to the east, with the oldest single strand of the NAF. (from Şengör et al. [2005]).

Geological studies show that the Aegean-NAF system can be understood as the result of two superposed systems: the propagating NAF that results from the westward motion of Anatolia and the extension of the Aegean related to subduction processes (fig. 3.2.6). According to Armijo et al. [2003], the NAF propagated into the Aegean at 1 Ma, increasing the activity of the Corinth Rift from about 1 mm/yr to about 10 mm/y. As a result, the NAF suppressed the extensional activity on its compressional side and increased it on the extensional side, applying at a large scale the concepts of linear elastic fracture mechanics (fig. 3.2.6c).

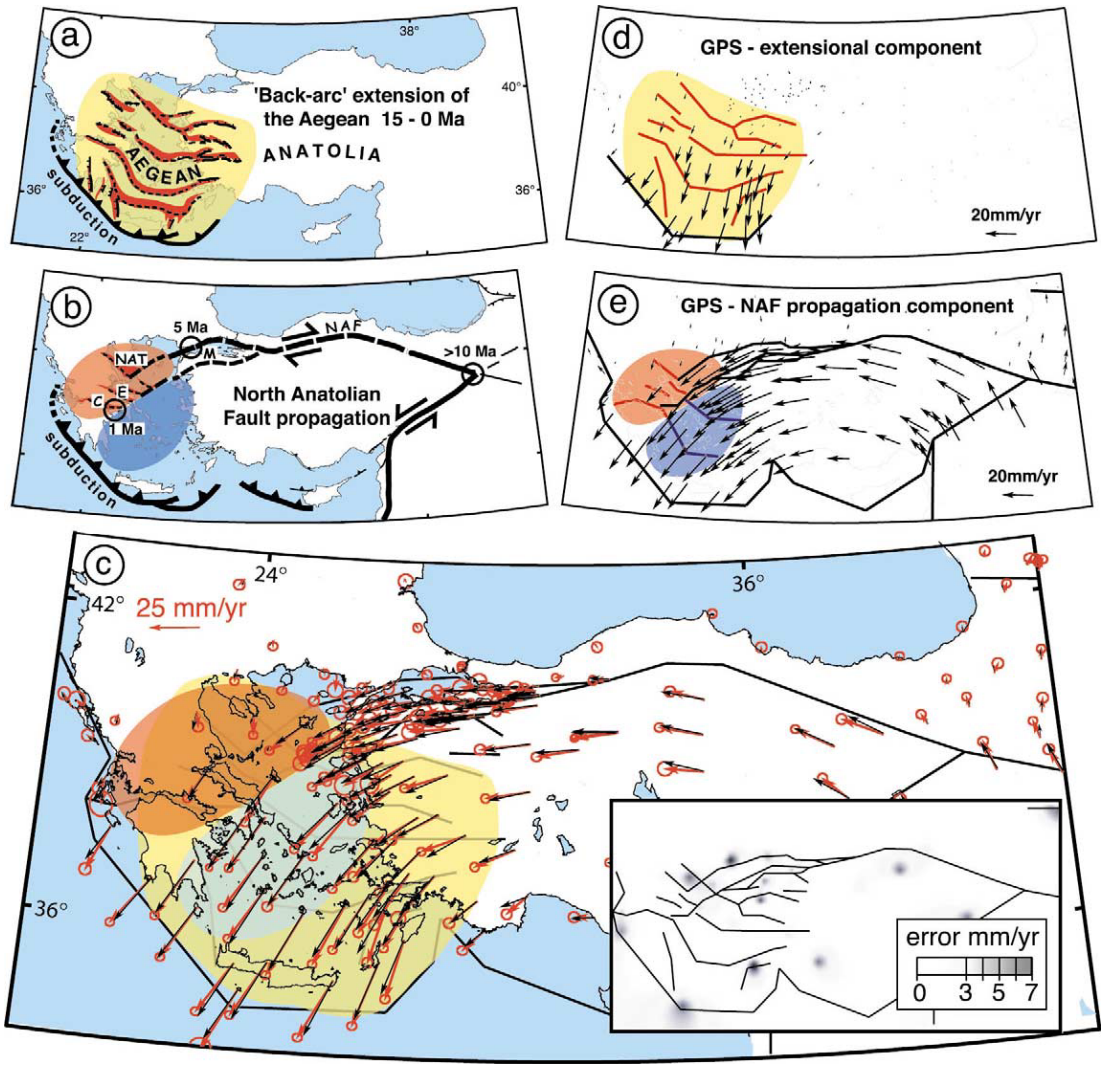

Figure 3.2.6. (a) The system of major structures that have been responsible for Aegean extension over the last 15 Myr. The origin of the extension is often attributed to 'back-arc' extension due to 'slab-pull' from the Aegean subduction. The main extensional structures are shaded in red and the overall zone where geological extension is observed is shaded in light yellow. (b) The evolution of the NAF. Circles indicate approximately where the first effects of the fault can be dated and the dates of arrival of the propagating fault are shown. The region where this zone is extensional is shaded light red and where it is contractional blue. The main extensional structures (shaded in plain red) are the North Aegean Trough (NAT), the Evvia fault system (E) and the Corinth Gulf (C). M denotes Marmara Sea. (c) The elements (black lines) used to model (black arrows) the GPS velocity vectors (red arrows). The 95% confidence ellipses (red) are shown. The red (superposed on yellow) shading indicates where the elements are required to have rapid opening to model the observations and the blue (superposed on yellow) where the rate of opening is modest. (d) The structures associated with the long-term extension in the Aegean (yellow) are shown in red. The black vectors are plotted at the same points as the GPS measurements and represent the part of the velocity field that can be attributed to Aegean extension alone. (e) The elements used to model the NAF propagation without the component due to Aegean extension are shown in black, blue and red. The vectors for central and eastern Turkey are consistent with the rates predicted by the Anatolia-Eurasia rotation. Red elements in the red shaded zone are associated with extension and blue elements in the blue shaded zone with contraction. Subduction is adjusted along the Hellenic subduction to absorb the extrusion associated with motion of the NAF. The red elements from north to south correspond to the North Aegean Trough, the Evvia fault system and the Gulf of Corinth. (from Armijo et al. [2003]).

The general model of extrusion of a rigid lithospheric plate, formerly proposed for the Tibet, has been used by several authors [McKenzie, 1972; Şengör, 1979; Barka, 1992; Şaroğlu et al., 1992] to explain the tectonics of Anatolia. In this model, the north-south Arabia-Eurasia

convergence and collision is accompanied by lateral extrusion of Anatolia towards the Aegean back-arc basin. Anatolia is then considered as a rigid lithospheric plate, moving between two conjugate transform faults (NAF and EAF) in the southwest. In this model, compression forces are supposed to apply only at the front of the Arabian indenter, the Aegean back-arc basin being considered as the free boundary of the Anatolian undeformed block (fig. 3.2.7). Compression in Eastern Turkey and extension in the Aegean are the boundary conditions permitting the lateral mass transfer of Anatolia from a squeezed region to a stretched one. In addition, the activation of the western NAF, as right-lateral guide of the westward escape of Anatolia, became necessary around the Late Miocene, when the mobility of the Pontides, in the northern block, decreased considerably, differently with respect to the free face to the south, due to the onset of the E-W Carpathian continental collision to the west [Şengör, 1993], as explained by the tectonic escape models [Mann, 1997] (fig. 3.2.8).

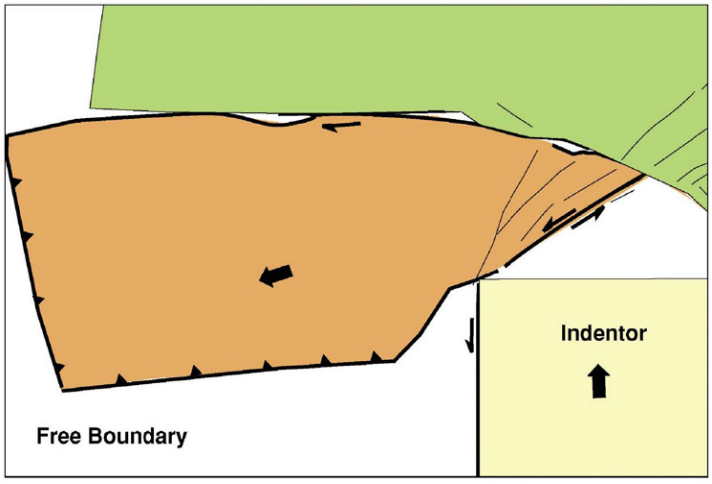

Figure 3.2.7. The Anatolian extrusion is similar to experiments in plasticine carried out by Peltzer *et al.* [1982]. The indentor is applied to a free boundary at the base and the system is free to move westward. As deformation evolves a left-lateral fault first appears in the east. It is then cross cut by a right lateral fault that propagates toward the free boundary in the west. (from Hubert-Ferrari et al. [2003]).

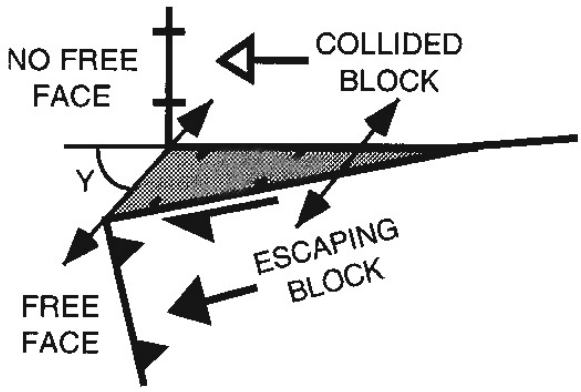

Figure 3.2.8. Tectonic escape models for formation of large transtensional basins. AngleY represents angular amount of reorientation for the escaping plate. Basins formed in shaded, triangular zone include both pull-apart and transform-normal extensional types. (from Mann [1997]).

Conversely, according to several Authors [eg., Doglioni et al., 2002; Mantovani et al., 2002; Faccenna et al., 2006], the westward escape of Anatolia does not result from a simple process of collision and incipient extrusion of a rigid block, but includes body forces inducing crustal-scale detachments. They argue that extension and strike-slip tectonics prevailed in Anatolia since the late Cenozoic and that these deformations are not consistent with the concept of compressional deformations resulting from the Arabia-Eurasia collision. Other doubts about the feasibility of the extrusion model are based on the fact that the Aegean Arc is moving faster (roughly 30 mm/y) than the Anatolian block (roughly 24 mm/y), apparently in contrast with the hypothesis that the deformation pattern of the Aegean zone is driven by the Anatolian westward push. Also, the westward Anatolian extrusion can be ruled out because plates velocity vectors increase from eastern Anatolia to the Aegean and Greece. According to these Authors, this contradicts the basic rule that the velocity field decreases moving away from the source area of the energy. Some authors [*e.g.*, Le Pichon and Angelier, 1979; Jolivet et al., 1994; Le Pichon et al., 1995] argued that the occurrence of extensional strain in the Aegean region during the lower-middle Miocene demonstrates that the tectonic evolution of this region cannot be taken as an effect of the westward escape of Anatolia, since at that time the western segment of the North Anatolian fault (NAF) was not formed yet. According to Faccenna et al. [2006], the breaking of the slab under the collisional belt may permit the lateral escape of material towards the west and the formation of the NAF, triggering, (1) the

acceleration of slab retreat to the west due to the increase in slab pull force there, and (2) the indentation of the continent in the collisional area (fig. 3.2.9).

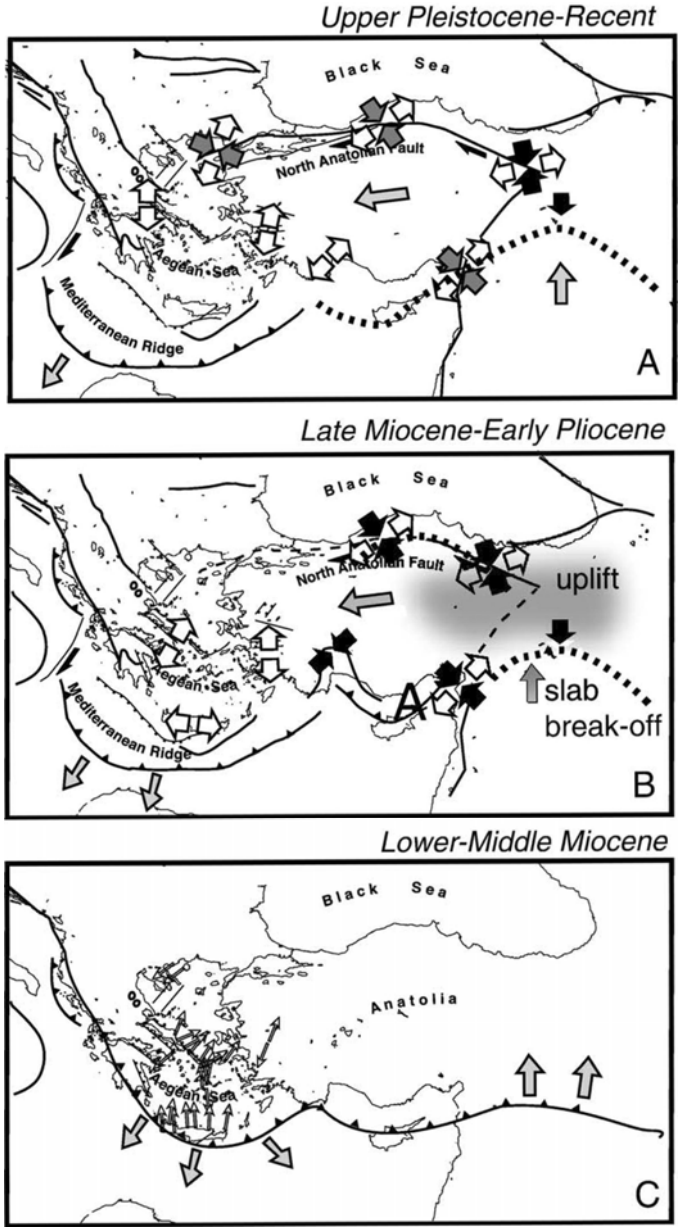

Figure 3.2.9. Tectonic evolution of the Anatolia–Aegean region after (A, Upper Pleistocene–Recent), during (B, Late Miocene–Early Pliocene) and prior (C, Lower Middle Miocene) to the formation of the NAF. The coast line is taken fixed for reference. Plate boundary is displaced accordingly to the amount of shortening and back-arc extension. Stretching directions shown in frame C are from [Jolivet et al., 2001]. Grey long arrows near plate boundary indicate the displacement. Black and white arrows indicate shortening (σ1 direction) and extensional regime (σ3 direction), respectively; double arrows set indicate σ1 and σ3 orientations for transpressional (black and white arrows) or transtensional (grey and white arrows) regimes. Shadow area represents the uplifted region of the Anatolia plateau. Dashed line indicates the broken slab. (from Faccenna et al. [2006]).

The Late Pleistocene to Present-day deformational pattern presents some differences with the previous stage. Along the NAFZ, the present-day state of deformation is dominantly strike-slip

right-lateral. Over et al. [1997] provide evidence for an early Quaternary change from regional transpressional to transtensional regime, preserving a NNW-trending orientation for the horizontal maximum stress axes. Geodetic data [*e.g.*, McClusky et al., 2000], earthquake focal mechanisms [Taymaz et al., 1992; Eyidogan and Barka, 1996] and structural analyses [Temiz et al., 1997] show widespread heterogeneous extensional regime also in south central Anatolia, with NNE and NW-trending extension axes.

3.2.2. Recent tectonic setting

Nowadays, the clear surface trace of the North Anatolian Fault Zone (NAFZ) extends from the Gulf of Saros, in the northern Aegean Sea, to the triple junction with the EAF, in Eastern Turkey, for about 1500 km (fig. 3.2.1), paralleling roughly the southern Black Sea shores with an upward-convex trajectory and keeping a fairly regular distance of some 100 km to the coast, connecting the Aegean with the East Anatolian high plateau. The NAFZ mostly follows the Intra-Pontide suture zone within Northern Anatolia and in few places it obliquely cuts and displaces it. To the east of the town of Bolu, the NAFZ is formed by a main single trace but, west of it, it splays into two main strands, the Düzce, to the north, and the Mudurnu, to the south, fault segments. Farther west, the NAFZ splays again into three major strands [Barka and Kadinski-Cade, 1988; Barka, 1992] that forms the pull-apart basins hosting the Marmara Sea [Wong et al., 1995; Le Pichon et al., 2001; Armijo et al., 1999; Okay et al., 1999] (fig. 3.2.1). Regional GPS networks measured present-day strain-rates in the northern part of the Anatolian block up to ca. 25 ± 5 mm/yr, with vectors oriented WNW in the easternmost region, E-W in the centre, and SW in the Aegean, and indicates that most of the present-day strain is accommodated along the northern fault strand at the Marmara Sea [Reilinger et al., 1997 and 2000; Straub et al., 1997; McClusky et al., 2000; Kahle et al., 1999 and 2000]. The geodetically determined Anatolia mean displacement approximately corresponds to a rigid rotation (internal deformation less than 2 mm/year) with an Euler pole located near the Nile delta [Le Pichon et al., 1997; McClusky et al., 2000] (fig. 3.2.1).

Since the Late Miocene-Pliocene (13-5 Ma) the NAFZ has accumulated a geologic displacement on the order of 85-120 km [Seymen, 1975; Şengör, 1979; Barka, 1981; Barka and Hancock, 1984; Westaway, 1994; Armijo et al., 1999; Hubert-Ferrari et al., 2002]. This displacement translates to long-term and short-term geologic slip rate of 0.5-0.8 cm/yr [Tokay, 1973; Seymen, 1975; Barka and Hancock, 1984] and 1.8 cm/yr [Hubert-Ferrari et al., 2002], respectively.

Limited documented geological slip-rates indicate the NAFZ slip rates with a large variability over various timescales, from 2 mm/yr up to 23 mm/yr (fig. 3.2.10). Although these values contain large uncertainties, the fact they are much lower than the present-day geodetic measurements suggests an acceleration of the deformation over time (or a low reliability in measurement and dating of geological offsets). According to some Authors the NAFZ presents a uniform amount of deformation all along the fault and has accumulated a total geologic displacement of 85 ± 15 km [Hubert-Ferrari et al., 2002] or of 75 ± 10 km [Westaway, 1994 and Armijo et al., 1999]. Conversely, according to Barka [1992], since the Early Pliocene, the NAFZ has accumulated a total geologic displacement of 40 ± 5 km, with decrease to 25 ± 5 km east of the Marmara Sea. Therefore, on the basis of the NAFZ age, the total displacements translate to geological slip rate ranging from 6.0 up to 23 mm/yr (1, 10 and 11 in fig. 3.2.10).

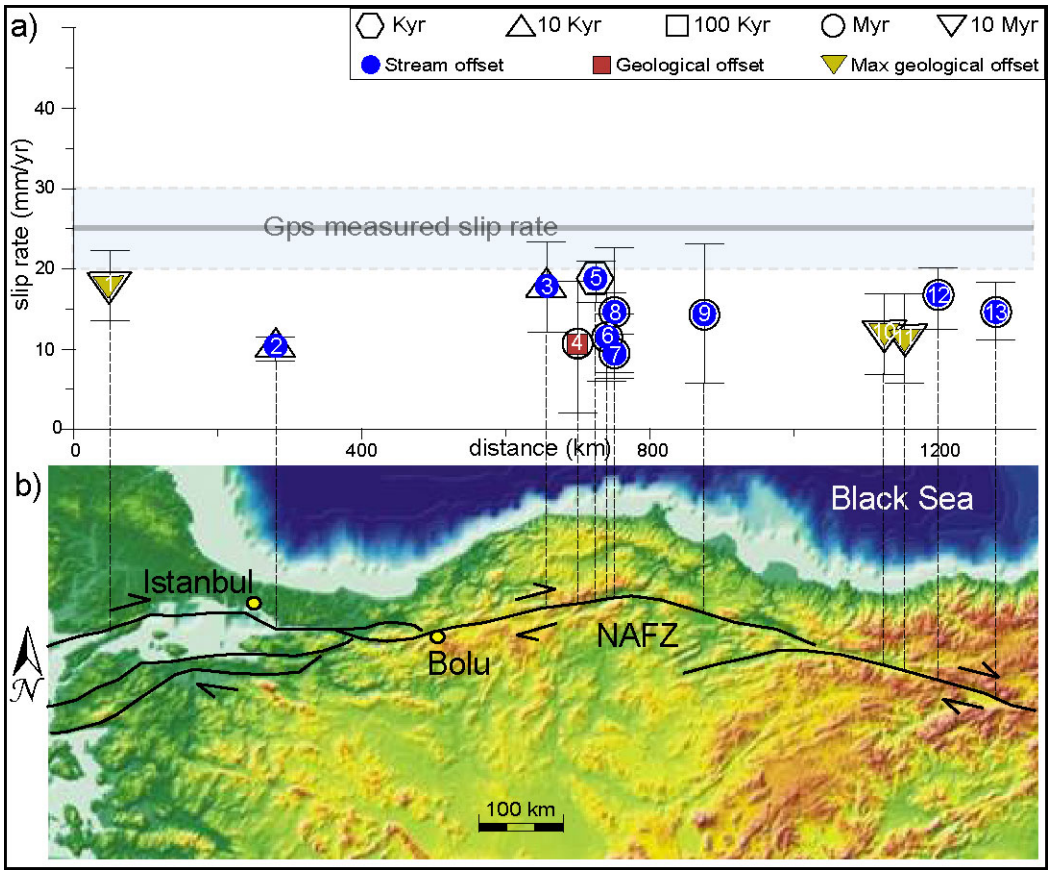

Figure 3.2.10. a) Slip rates distribution along the North Anatolian Fault Zone (NAFZ). Different symbols are used on the basis of the time-scale and type of measured offset. Thin bars indicate uncertainties of the measurements. b) Location of the slip rate measures along the NAFZ. Numbers refer to slip rates from: (1) Armijo et al. [1999]; (2) Polonia et al. [2004]; (3) and (5) [Hubert-Ferrari et al., 2002]; (4) Dhont et al. [1998]; (6) to (9), (12) and (13) Erinç [1953], Gaudemer et al. [1989], Barka and Gulen, [1989], Huber-Ferrari et al. [2002] and Şengör et al. [2005]; (10) and (11) Irrlitz [1972], Seymen [1975], Tatar [1978], Barka, [1992], Westaway [1994] and Hubert-Ferrari et al. [2002].

The punctual long-term (Pliocene-Pleistocene) and short-term (Holocene) slip rates show a high variability. These are reported in figure 3.2.10 and range between: 7 and 23 mm/y [Erinç, 1953; Gaudemer et al., 1989; Barka and Gulen, 1989; Huber-Ferrari et al., 2002; Şengör et al., 2005] from deflected Early Pliocene river system (6-9 and 12-13 in fig. 3.2.10); 10.3 ± 8.2 mm/yr from a Pliocene-Middle Pleistocene offset basin (4 in fig. 3.2.10) [Dhont et al., 1998]; 10 ± 1.5 mm/yr from a 10,200 yr old underwater stream deflection (2 in fig. 3.2.10) [Polonia et al., 2004]; 18.4 ± 2.6 mm/yr and 17.8 ± 5.3 mm/yr from 10,000-12,000 yr old and 1600-4000 yr old stream terrace offsets, respectively (4 and 6 in fig. 3.2.10) [Hubert-Ferrari et al., 2002].

The data collected suggest that the rate of motion of NAFZ has being changing both in time and space during its history from 6.0 mm/yr to 20-30 mm/yr. Yet, the scientific community

proposes two different reasons for this. 1) Armijo et al. [1999] and Hubert-Ferrari et al. [2002] accepts as true the Pliocene age of the western part of the NAFZ and, since they hypothesizes the westward propagation of the fault that started from its Late Miocene easternmost part [Hubert-Ferrari et al., 2003], interpret the western, higher short-term slip rates as due to a recovery strain. 2) Conversely, Şengör et al. [2005], since they consider all the North Anatolian transform margin coeval (13-11 Ma old), hypothesize that, starting from a partitioned and wider deformation zone, the deformation become localized (along the present NAFZ) at different times along its strike. Under this light, the transform margin presents a diachronic acceleration of the slip rate, slower to the west with respect to the east (fig. 3.2.11).

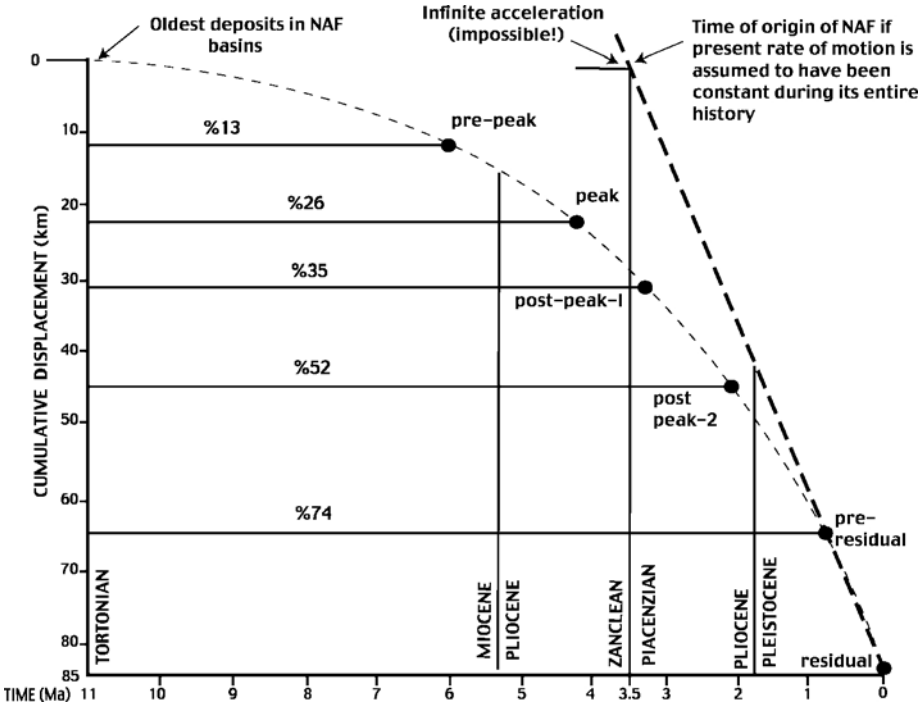

Figure 3.2.11. Plot of cumulative offset against time since the origin of the NAFZ deduced from its associated basins. Also plotted is the present rate of motion of the fault, which is approximately 2.5 cm/year. The backward linear projection in time of the present rate, shows that the present cumulative offset would have accumulated in 3.5 Ma. The time of the origin of the NAFZ (11 Ma) imply an acceleration of the slip rate. (from Şengör et al. [2005]).

The present-day high strain rate of the NAFZ is seismically accommodated by a large number of earthquakes [Ambraseys, 1970 and 2002; Ambraseys and Finkel, 1995; Canıtez and Üçer , 1967; Orgülü and Aktar, 2001; Taymaz et al., 1991; Harvard; USGS]. Seismicity along the

active segments of the NAFZ is characterized by frequent moderate to large earthquakes (M>7), most of which accompanied by surface ruptures during the last century [*e.g.*, Angelier et al., 1981; Barka and Kadinski-Cade, 1988; Barka, 1992; Westaway, 1994], with focal mechanisms that show essentially pure right-lateral strike-slip solutions [Canıtez and Üçer, 1967; McKenzie, 1972; Reinecker et al., 2004, see http://www.world-stress-map.org] (fig. 3.2.12).

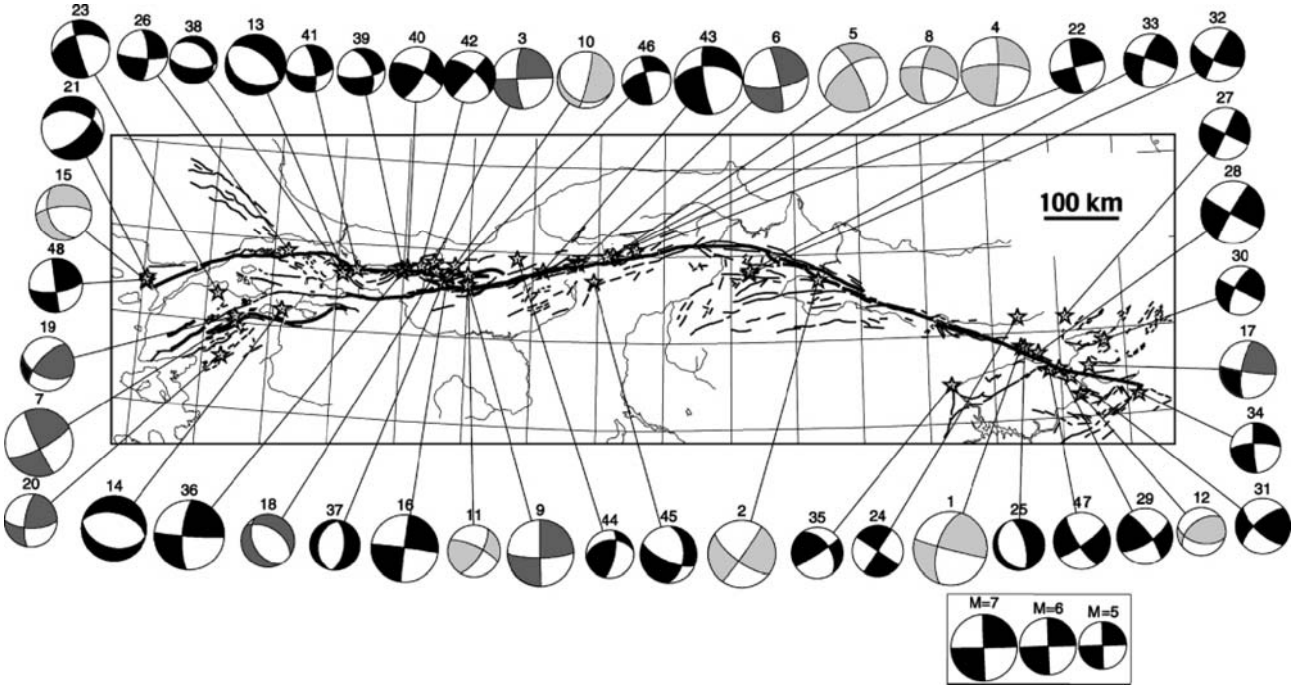

Figure 3.2.12. Focal mechanism solutions of NAFZ earthquakes. Instrumental records with Ms ≥ 5 from 1939 to 2003. Fault plane solutions are shown as lower hemisphere stereographic projections with compressional quadrants shaded. Solutions with black compressional quadrants are the most reliable ones determined by wave-form modeling techniques. Solutions with darker gray compressional quadrants are those determined by visual examination of seismograms. Solutions with lighter gray compressional quadrants are those obtained by plotting readings from Bulletins, but are compatible with the surface characteristics of the fault. (from Şengör et al. [2005]).

During the 20th century, the North Anatolian fault has produced a sequential westward progression of M_W >6.7 earthquakes along different sections of the fault. This sequence begun with the 1939 M 7.9 earthquake, which produced about 350 km of ground rupture along the eastern North Anatolian fault, and ended with the most recent 1999 Izmit sequence that occurred along the northern strand of the NAFZ, east of the Marmara Sea. Stein et al. [1997] showed that the observed ruptures were brought closer to failure due to the earthquake-induced changes in stress by the preceding shocks on adjacent fault segments (fig. 3.2.13).

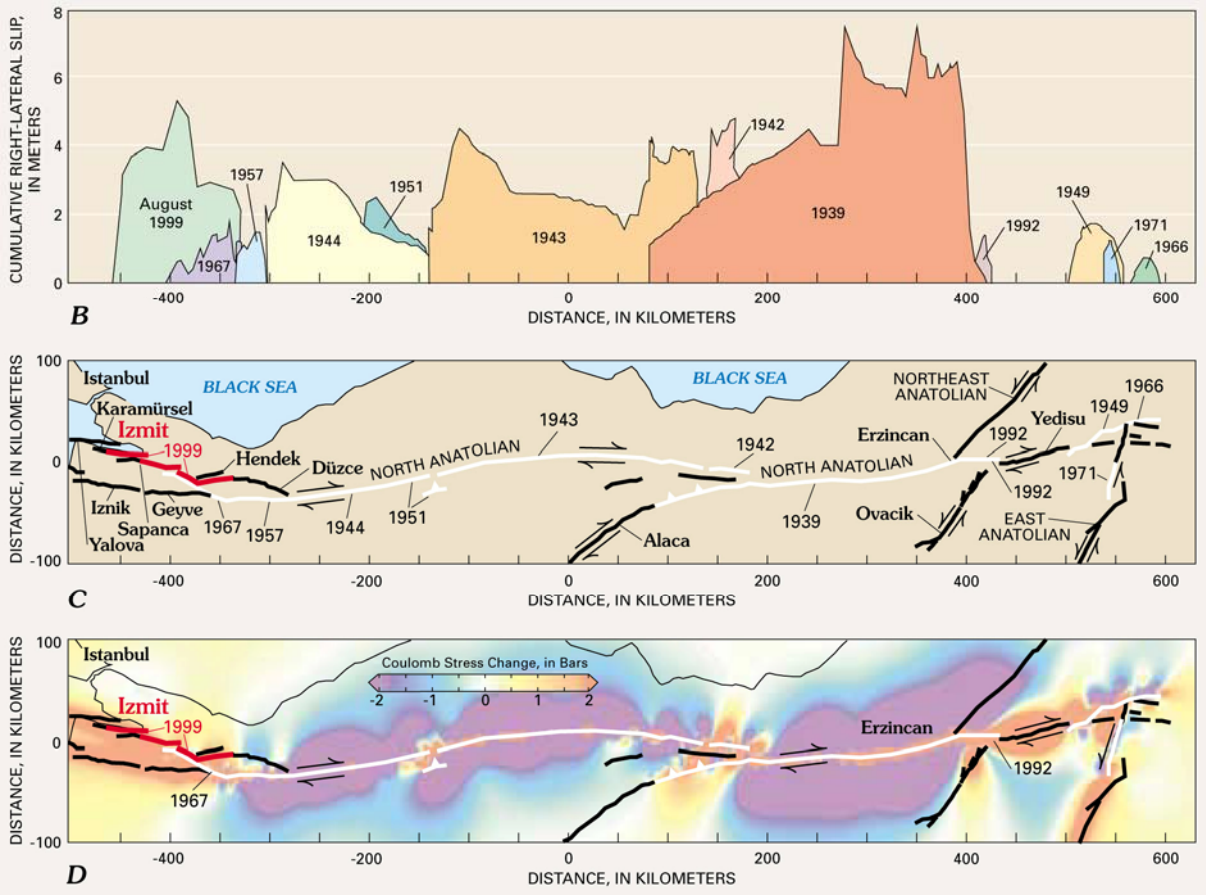

Figure 3.2.13. B) and C) The westward progression of 20th century earthquake ruptures is associated with fault slip of 2-6 m in each event, with 4 m as average. D) Stress build-up on the North Anatolian faults associated with the 1939-1967 westward progression of earthquakes and the contribution of steady stress accumulation. The August 17, 1999, ground rupture is shown in red. Faults are projected relative to pole of rotation of the Anatolia plate. Modified from Stein and others [1997]. (from USGS [2000]).

The 1999 Izmit sequence is composed by two highly damaging earthquakes (fig. 3.2.14) that follow two large events that ruptured the southern strand of the NAFZ along the Mudurnu valley in 1957 (Ms 7.0 [McKenzie, 1972]) and 1967 (Ms 7.1 [Ambraseys and Zatopek, 1969; Pinar et al., 1996]). The first of these earthquakes occurred on 17 August and struck the Izmit region, west of the Marmara Sea. This Mw 7.4 [USGS] earthquake nucleated at a depth of 13 km and its focal mechanism [Harvard CMT] is consistent with right-lateral movement along an E-W strike-slip fault (fig. 3.2.14). It produced more than 150 km of surface ruptures organized in five major fault sections (Hersek, Karamursel-Golcuk, Izmit-Sapanca, Sapanca-Akyazi and Karadere sections), with dextral offsets exceeding 5 m [Barka, 1999; Barka et al., 2000 and 2002] (fig. 3.2.14 and 3.2.15).

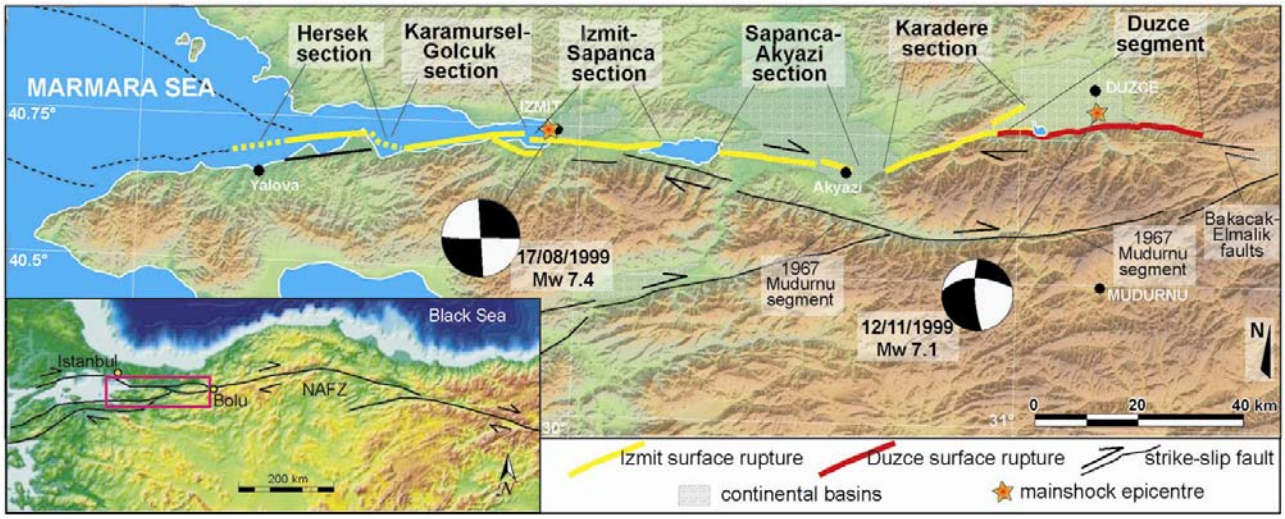

Figure 3.2.14. The Izmit and Düzce earthquake ruptures [modified from Akyuz et al. [2002]. Epicenter location (stars) and focal mechanism solutions from Harvard CMT. Inset locates the region of the NAFZ affected by the 1999 seismic sequence. (see lower left inset for location of the area).

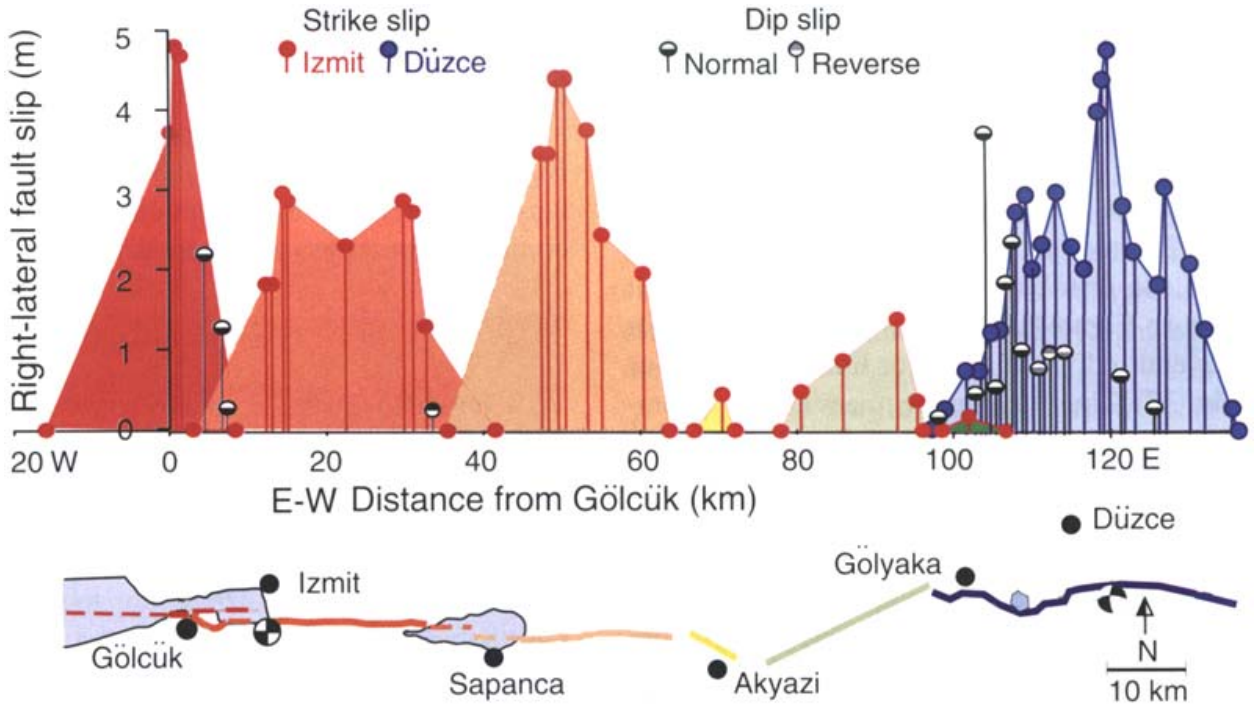

Figure 3.2.15. Slip distribution along the rupture zones. (from Aydin and Kalafat [2002]).

The number of large historical earthquakes attributed to the NAFZ places this fault among the most active strike-slip structures worldwide [Ambraseys, 1970; Ambraseys and Finkel, 1995; Ambraseys, 2002] (fig. 3.2.16) and testifies that the present-day high deformation rate is

seismically accommodated with rates of 20 ± 10 mm/yr (from seismic moment release over the past 100-400 years [Jackson and McKenzie, 1988; Westaway, 1994]).

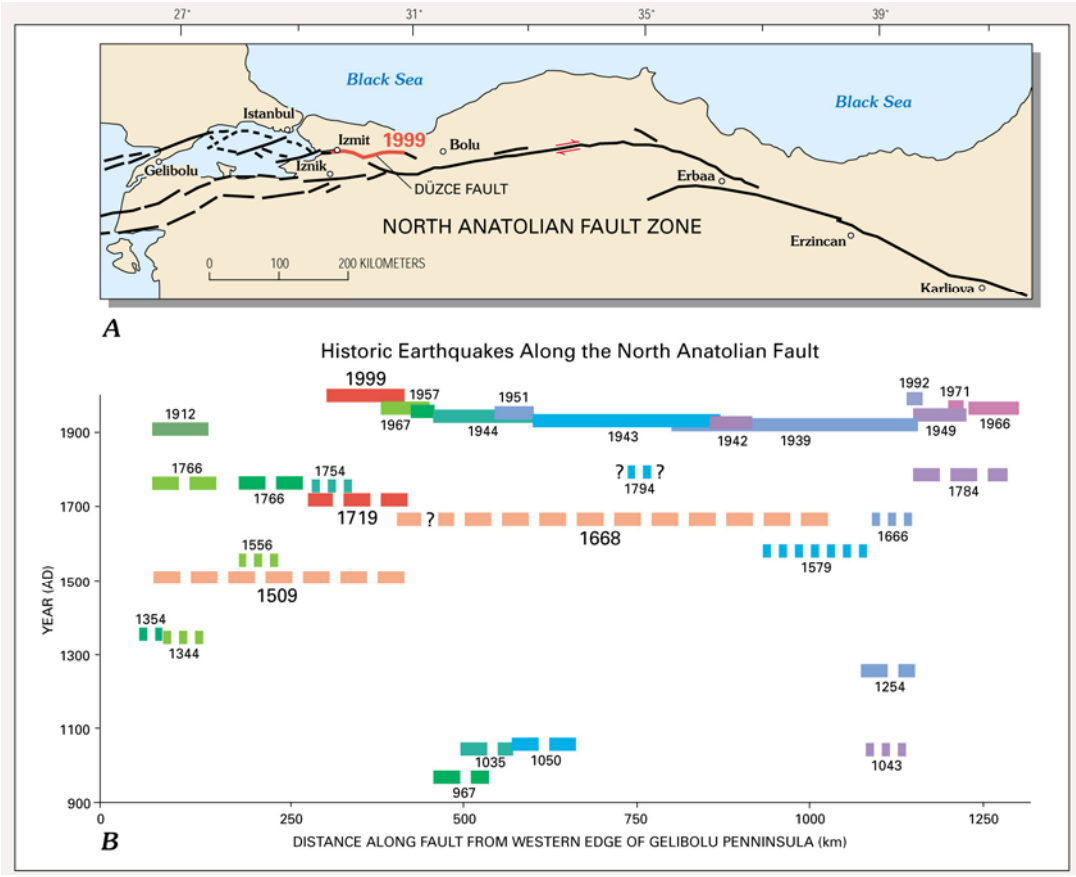

Figure 3.2.16. A) Strip map showing the 1500-km-long North Anatolian fault. The section of the fault that ruptured to the surface during the 1999 Kocaeli earthquake is shown in red. [from USGS, 2000]. B) Historical earthquakes located along the fault where they are believed to have ruptured the ground surface. Solid lines indicate an earthquake known to have ruptured the ground, long-dashed lines indicate highly probable surface-rupturing events, and short-dashed lines are shown when the earthquake is believed to have ruptured the ground but that interpretation of the historic record has less certainty. [Compiled from Ambraseys, 1970; Ikeda et al., 1991; Ambraseys and Finkel, 1995; Barka, 1996; Stein et al., 1997]. (from USGS [2000]).

The historical record does show that several ground-rupturing earthquakes had occurred in close succession in the past, as with the sequences of events in the mid-eighteenth, fourteenth, and eleventh centuries. Such record does not support the theory that the seismic behavior of the North Anatolian fault in the 20th century is a repetition of the pattern of earlier centuries, even if the earthquake activity between 1719 and 1912 seems to have migrated generally westward. The 1999 rupture appears to be similar to the 1719 rupture, while before 1719, the same section of the fault slipped as part of a longer rupture. There is no record in the 20th century of an event similar to the one that produced the long rupture in 1668. Because few populated centers exists even nowadays

in the central portion of the fault, the lack of seismic record may be caused by this and gaps in the historic record of earthquakes may simply indicate that there is no record of the seismicity.

3.3. Study area: The Düzce fault segment (Ms 7.1, Nov. 1999) of the NAFZ

The increased seismic potential of the Düzce fault was recognized well before 1999 by Barka and Erdik [1993], who considered this fault the possible source of a near-future earthquake. Actually, three months after the Izmit event, on 12 November 1999, the Mw 7.1 Düzce earthquake [USGS, KOERI] occurred, likely triggered by the previous one [Parson et al., 2000; Muller et al., 2003, Utkucu et al., 2003] (fig. 3.3.1).

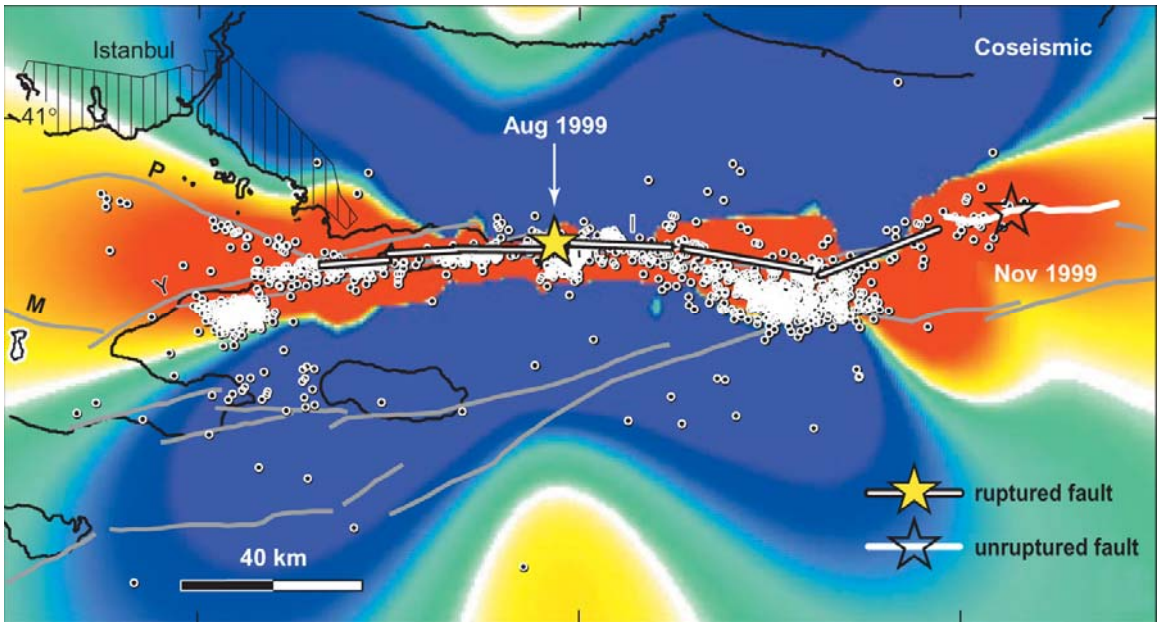

Figure 3.3.1. Coulomb stress map after the Izmit M_w = 7.4 (1999 August 17) earthquake. Red and blue colours indicate regions of increased and decreased Coulomb stress, respectively. White dots indicate locations of Izmit aftershocks. The occurrence of the 12 November Düzce earthquake is associated with stress increases caused by the main rupture (first 12 days from IZINET [Ito et al., 1999]), such as Izmit aftershocks and the Yalova cluster southeast of "Y,". Faults: Y-Yalova, P-Prince's Islands, M-Marmara, I-Izmit. (from Parson et al. [2000]).

The Düzce earthquake nucleated at a depth of 10-15 km [CSEM, European-Mediterranean Seismological Centre; Tubitak, Marmara Research Centre]; the focal mechanism solutions show almost pure, dextral strike-slip movement on an E-W nodal plane, dipping, depending on the solution, 54° to 73° to the north, with a rake between 184° and 167° (figs. 3.2.14 and 3.3.2; tab.3.3.1).

Source	E°	N°	Depth (km)	Mw	Strike °N	Dip°	Rake°	Mo (Nm)
USGS	31.161	40.758	19.0	7.1	269	73	177	5.6 1019
HVD	31.250	40.930	18.0	7.2	268	54	167	6.7 1019
CSEM	31.161	40.758	15.0	7.0	282	74	170	4.1 1019
OBN	40.758	31.161	15.0	7.3	260	53	175	9.1 1019
ERD	31.21	40.79	11.0	7.2	-	-	-	-
GFZ		-	-	7.1	264	64	184	4.6 1019
TUBI	31.16	40.83	9.6	-	-	55	-	-

Table 3.3.1. Parameters of the 1999 Düzce earthquake compiled from the following sources: UGGS: USA Geological Survey, HVD: Harvard University, CSEM: European-Mediterranean Seismological Center, OBN: Obninsk Seismological Observatory, Obninsk, Russia, GFZ: GeoForchungsZentrum Postdam, ERD: Earthquake Research Department (Disaster Affairs, Ankara), TUBI: TUBITAK-MAM. (from Çakir [2003a]).

The pattern of aftershocks, recorded between 12/11/99 and 20/11/99 by the TÜBİTAK-MAM local network, is organized in clusters that are all located north of the surface trace of the Düzce fault [Özalaybey et al., 2000; Milkereit et al., 2000; Çakir et al., 2003a] (fig. 3.3.2). This earthquake produced right-lateral surface ruptures for a total length of ca. 40 km and a maximum dextral offset of 5 m [Akyuz et al., 2000 and 2002]. The ratios of average and maximum slip to surface rupture length along the Düzce fault were much higher than in any previous historic earthquake along the NAF and not consistent with worldwide empirical relationships [Wells and Coppersmith, 1994]. The distribution of aftershocks suggests that some subsurface slip might extend eastward past the ruptured surface trace, but this alone can not explain the high slip-to-rupture-length ratio. Conversely, the ratios of average, maximum slip and surface rupture length to moment magnitude of the Düzce fault were consistent with the empirical relationships [Wells and Coppersmith, 1994]. According to Ayhan et al. [2001] the Düzce earthquake was effectively part of a composite rupture starting with the Izmit event, since the slip magnitude was more consistent with the combined rupture length of ~160 km.

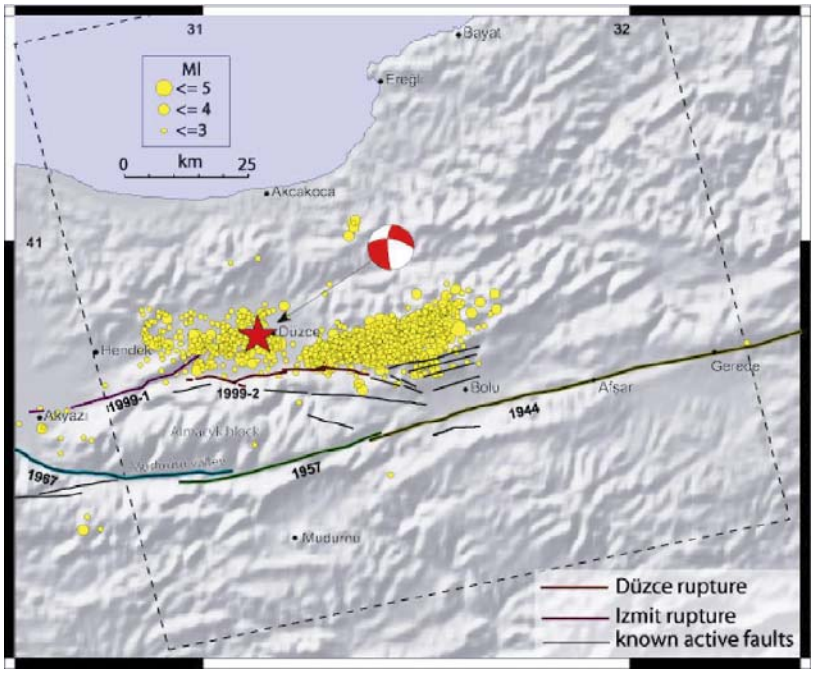

Figure 3.3.2. The 1999 and previous earthquake's breaks and neighboring active faults. Star denotes the epicenter of main shock of the Düzce earthquake with the focal mechanism solution from Harvard CMT. Yellow circles are aftershocks recorded between 12/11/99 and 20/11/99 by the TÜBİTAK-MAM network [Özalaybey et al., 2000]. The background DEM image is from GTOPO30. Dashed box shows the location of the ERS Interferograms. (from Çakir et al. [2003a]).

The Düzce fault segment has an average E-W trend and a clear geomorphic expression for about 40 km. It separates the Paleozoic-Eocene formations of the Almacik block to the south from the Quaternary Kaynasli and Düzce basins to the north (fig. 3.3.3). The Düzce Basin, interpreted by Aydin and Kalafat [2002] as a composite pull-apart basin, contains a 260m-thick alluvial-lacustrine deposits that sits mainly on Eocene volcanogenic flysch [Komut, 2005] (fig. 3.3.3).

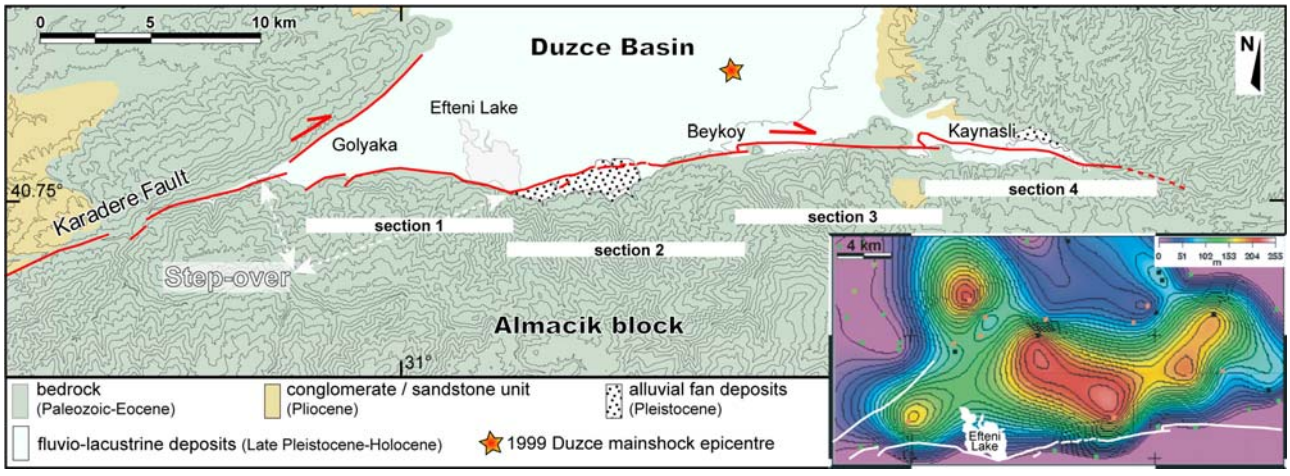

Figure 3.3.3. Simplified geological map of the Düzce area [modified from Herece and Akay, 2003] and trace of the Düzce fault with sections (modified from Akyuz et al. [2000]). Contour interval 100 m. Inset show the thickness of the Düzce basin infill. Contour interval 10 m. (from Komut et al. [2005]).

The basin infill is formed by Late Pleistocene-Holocene, Gilbert deltas sediments that overlie unconformably Pliocene-Early Pleistocene alluvial-lacustrine sequence [Emre et al., 1998].

Although with internal differences, the overall long-term morphological expression of the Düzce fault depicts a single and continue structural element that produces uplift of the range, to the south, with respect to the plain, to the north.

In the western part of the basin, the E-W Düzce fault splays out from the WSW-ENE trending Karadere section, that represents a restraining bend of the Izmit Fault. According to Lettis et al. [2002], this western boundary of the Düzce fault segment forms a complex right releasing step-over with the Karadere section that presumably represented a barrier to the August rupture propagation. This releasing zone controls the present-day Düzce Basin depocentre, that coincides with Lake Efteni (fig. 3.3.3). The eastern termination of the Düzce fault is not clearly defined and, according to Barka and Erdik [1993], it may join the eastern single trace of the NAFZ *via* a right-releasing step-over, involving the WNW-ESE trending Bakacak and Elmalik faults (fig. 3.2.14).

As already mentioned, in this part of the North Anatolian Fault, the Düzce fault to the north and the Mudurnu fault to the south represent the two main strands (fig. 3.2.14). According to Ayhan et al. [1999 and 2001], the Düzce Fault accommodates 33% to 50% (*i.e.*, up to 10 mm/yr) of the present-day GPS strain of the NAFZ. Geological slip rates obtained from the analysis of offset geomorphic markers of the Düzce and the Mudurnu faults are not known. Conversely, some slip rates are derived from paleoseismological studies are unknown for the Düzce fault and 11 ± 5 mm/yr for the Mudurnu fault [Ikeda et al., 1991; Yoshioka et al., 1991; Palyvos et al., submitted].

In general, the 40 km long coseismic rupture is simple and narrow with a deformation zone 0.5 to 5 m-wide with local exceptions where the width reaches 50 m. The coseismic ruptures do not exactly run at the mountain-piedmont interface, but affect both basin infill deposits and bedrock with a slightly northward-convex trajectory. Due to the strike variability of the rupture, transpressional and transtensional structures formed along the fault trace [Akyuz et al., 2002; Hartleb et al., 2002]. On the basis of geometry and the coseismic slip distribution, Akyuz et al.

[2002] divided the entire Düzce rupture into four sections (fig. 3.3.3), each of them showing a symmetric slip tapering off towards both ends. The westernmost sections (1 and 2, fig. 3.3.3) are separated by a releasing bend with a significant normal component of displacement, whereas the eastern sections (2, 3, and 4, fig. 3.3.3) are separated by two, 1-km wide, transpressional left step-overs [Duman et al., 2005], which, as would be expected for such small-scale features, did not represent in 1999 a barrier to the rupture propagation [Barka and Kadinski-Cade, 1988; Wesnousky, 1988; An, 1997; Kase and Kuge, 2001; Harris and Day, 1993 and 1999]. Interestingly, the westernmost part of the Düzce fault segment slipped also during the August earthquake, but with only up to 25 cm horizontal and 10 cm vertical surface offset (fig. 3.2.15) [Hartleb et al., 2002; Emre et al., 2003a].

Several Authors provided models of the coseismic Düzce fault plane at depth by means of inversion methods of geodetic [Ayhan et al., 2001; Burgmann et al., 2002; Çakir et al., 2003a], seismological [Tibi et al., 2001; Umutlu et al.,2004; Birgoren et al.,2004] or joint data [Bouin et al., 2004]. GPS coseismic data shows ~3 m average right-lateral offset at the surface, and InSAR data shows ~0.4 m average dip-slip basin dislocation, 5 km north of the fault trace. Modeled slip distribution at depth show consistently that the earthquake nucleated near the bottom center of the northward dipping rupture and propagated bilaterally east and west and that the right-lateral Düzce rupture was simple and concentrated in space, with a single, round-shaped, 10-25 km-wide, 6-8 meters maximum slip asperity, located in the eastern part of the fault (*e.g.*, fig. 3.3.4.).

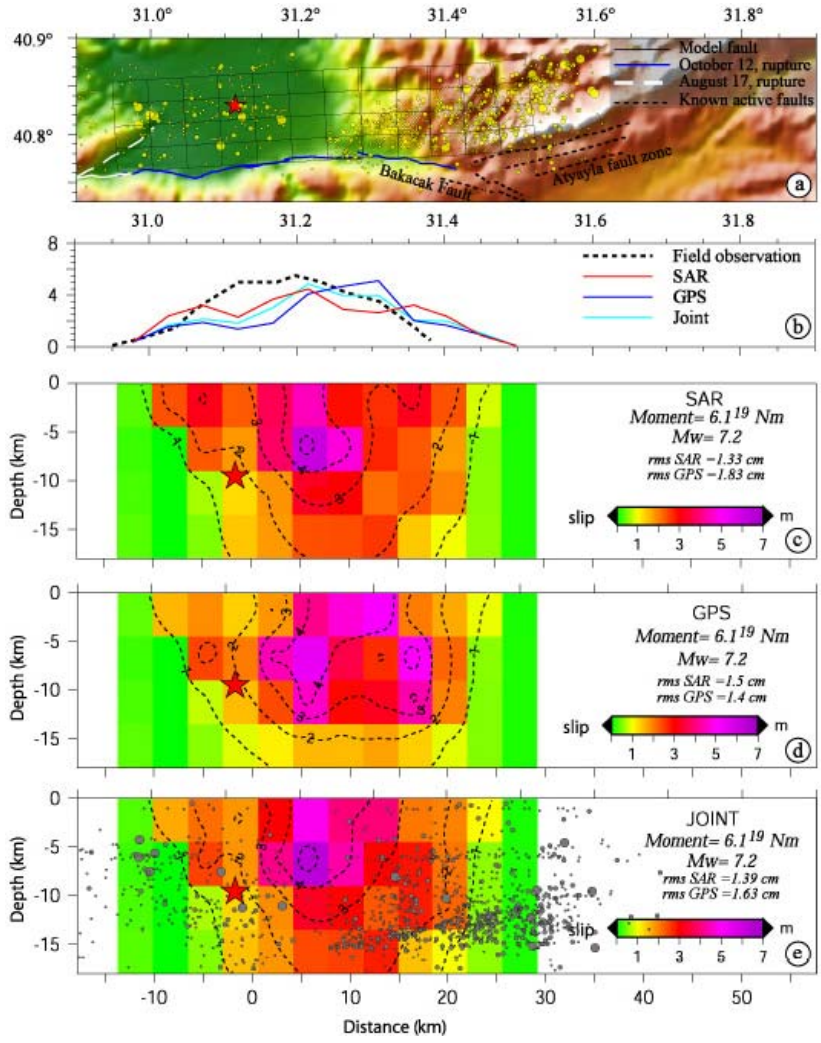

Figure 3.3.4. The Düzce earthquake fault trace, the coseismic surface slip and the modelled slip distribution at depth with single-fault-rupture geometry. (a) Shaded topographic map with simplified fault trace and the model fault projected to the surface. The model fault has 48 patches (4 km x 4.5 km) and dips 62° to the North. Locations of mainshock (red star) and of aftershocks (yellow circles) are reported. (b) Surface right-lateral slip projected along the fault trace observed in the field is shown with a black dashed line. For comparison, surface slip predicted by SAR, GPS and joint inversions are also shown. (c) The InSAR model. Red star represents main shock hypocenter with the aftershocks shown with gray circles. (d) The GPS model (data from Ayhan et al. [2001]. (e) The slip distribution derived from joint inversion of InSAR and GPS data. (from Çakir et al. [2003a]).

The available geodetic data set have been explained by models with either single or multiple-fault-rupture geometry within the uncertainty level of the geodetic data set. Inadequate coherence of the InSAR data and lack of GPS points (fig. 3.3.5) particularly in the near field allow models with both types of rupture geometry to fit the geodetic data within the acceptable limit of error.

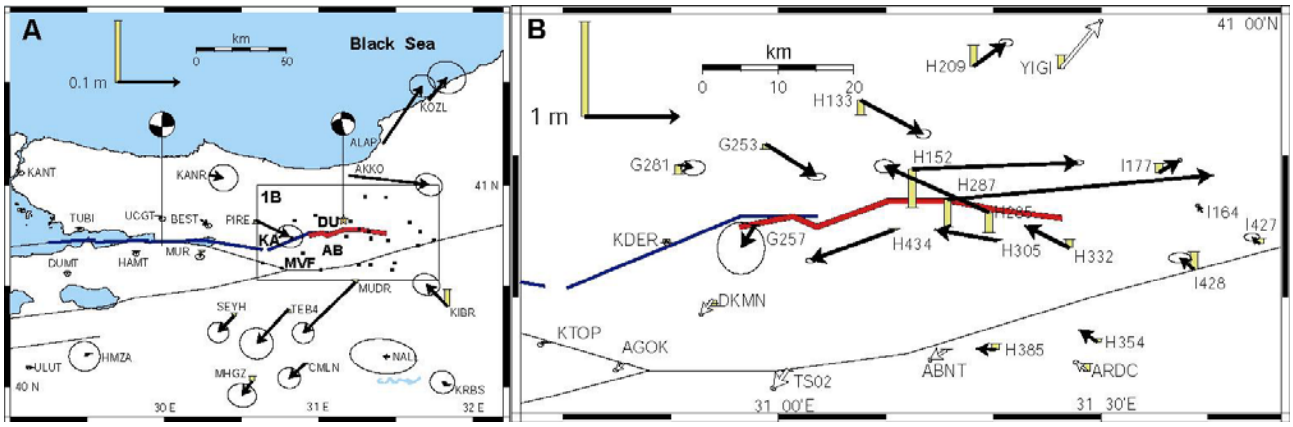

Figure 3.3.5. Fault map with GPS-measured Düzce earthquake surface displacements. Arrows tipped with 95% confidence ellipses are horizontal motions and flat-tipped yellow bars indicate the vertical displacements. (A) Regional view with focal mechanisms [Harvard CMT] of the 1999 Izmit and Düzce earthquakes. KF, Karadere fault segment; DF, Düzce fault; MF, Mudurnu fault segment; AB, Almacik block. Blue line follows the Izmit earthquake rupture, the red line indicates the Düzce rupture surface trace. Boxed area is shown in close up in (B). Open arrows in (B) are from Ayhan *et al.* [2001]. (redrawn from Burgmann et al. [2002]).

Bürgmann et al. [2002] inverted the same InSAR and GPS data jointly for subsurface slip using single-fault-rupture and concluded that the geodetic data rule out a near-vertical geometry of the Düzce fault. In fact, they propose a geometry of the fault plane with 54° north dip and found a slip patch with 5m maximum in the eastern part, similar to that found by Ayhan et al. [2001] who made use of GPS data only. The low-quality InSAR data show that the fringes, in the southern part of the fault, trend mainly E-W with low gradient, those in the north have a circular shape with high gradient. This apparent asymmetry suggest that the fault dips to the north and the displacement is not pure dextral-slip (fig. 3.3.6).

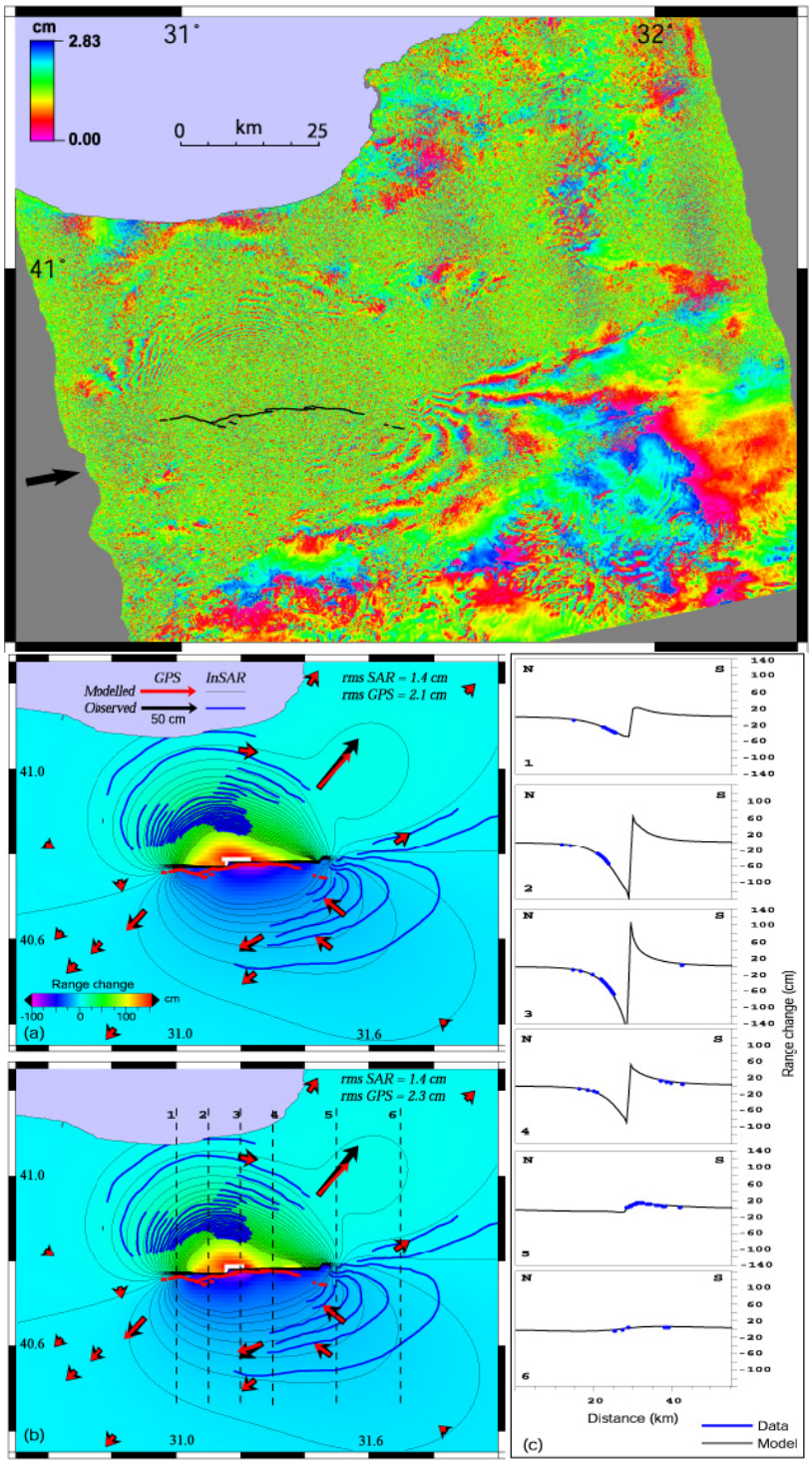

Figure 3.3.6. Comparison of the observed data and the models with a multiple-fault-rupture geometry derived from joint inversion of the GPS and InSAR data. Top) Interferogram of the coseismic deformation. Correlation is completely lost in the flat Düzce plain and around the Almacık block, whereas is preserved mainly in the south-eastern and in the north-northwest areas of the surface rupture. (a) Model with two faults intersecting at 6 km of depth. Background color map shows the modelled range change. Model fringes (thin gray lines) are contoured at every 2.83 cm to facilitate comparison with the observed fringes (thick blue lines). Black and read arrows show horizontal component of coseismic GPS vectors and modelled vectors, respectively. (b) Model with two faults intersecting at 8 km of depth. (c) Observed (blue) and modelled (black) profiles of range change across the fault along the lines shown in b. See Figure 4.9 for corresponding model of slip distribution at depth. (from Çakir et al. [2003a]).

To determine an optimum fault dip the InSAR and the GPS data are inverted separately and jointly. The geodetic data set is inverted for uniform slip with varying dips and the optimum dip angle for the two data sets is found to be 62°. An overall optimum rake is also sought using the same approach above and found to be 10° [Çakir et al., 2003a]. However Çakir et al. [2003a] demonstrates that a composite fault rupture encompassing a vertical Düzce fault can explain the geodetic observations reasonably well, too (fig. 3.3.7). Both GPS and InSAR data suggest that normal slip is restricted to the shallow portion of the rupture.

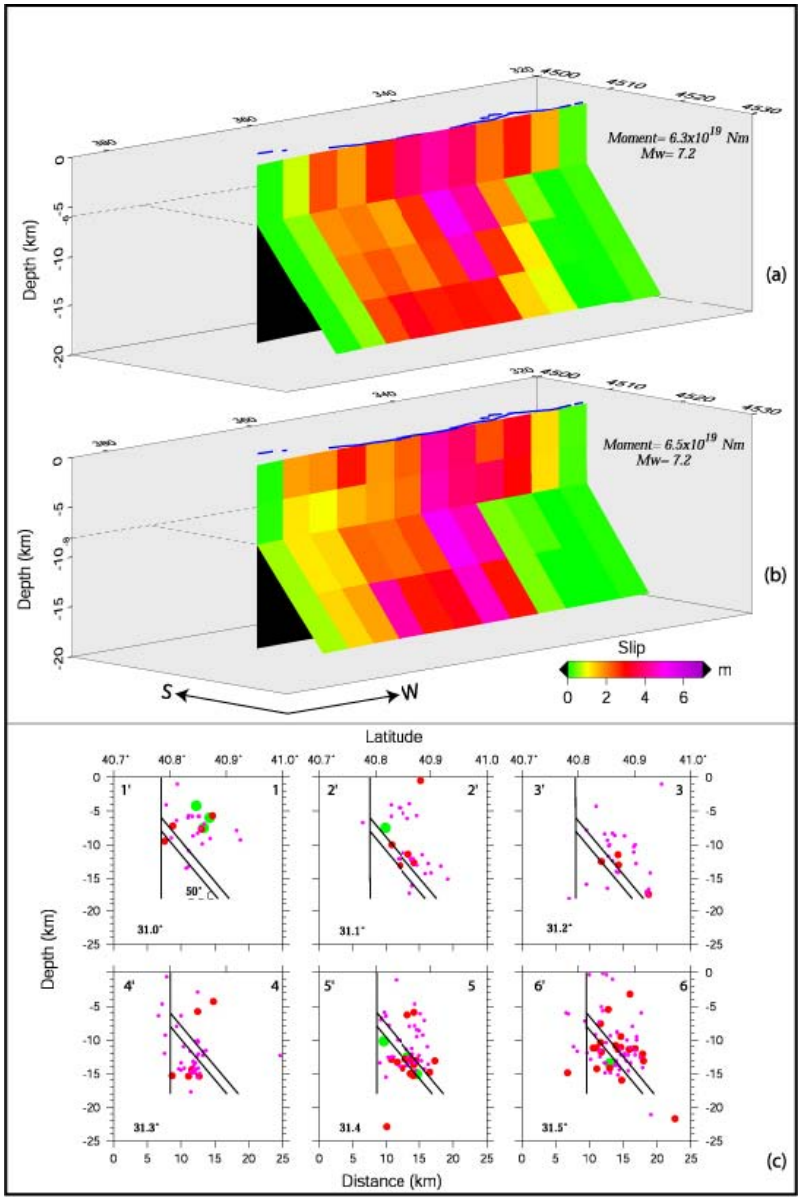

Figure 3.3.7. 3D perspective views of the fault models with slip distribution on two intersecting fault planes (one vertical one inclined). View is from NE towards SW. The intersection depth is 6 and 8 km in the first (a) and second (b) model, respectively. Blue lines are the surface rupture. (c) Cross sections showing the faults both in (a) and (b) in relation to one month aftershock distribution at depth. (from Çakir et al. [2003a]).

Although Turkey has one of the richer records of historical seismicity in the Mediterranean, no clear evidence for historical earthquakes produced by the Düzce segment of the NAFZ during the past centuries has been found. This is probably due to the scarce density of population and lack of cultural settlements in historical times in the Düzce region. The only historical earthquakes that are known to be close enough to be potentially associated to the Düzce fault are: AD1719, AD1878, AD1894, and AD967 [Ambraseys and Finkel, 1995; Ambraseys, 2002] (fig. 3.3.8). Interestingly, local people living near the eastern part of the Düzce fault recall their grandparents telling them about an earthquake at the end of the 19th century, producing ground ruptures exactly where these occurred in 1999.

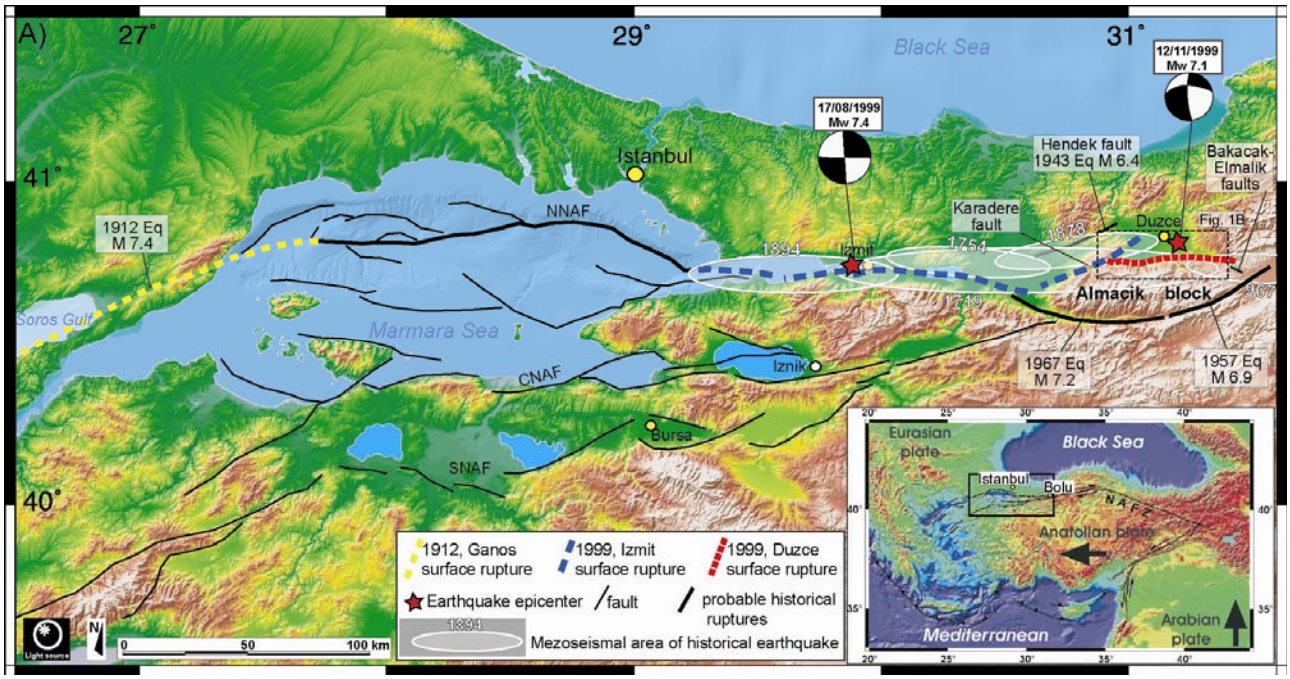

Figure 3.3.8. Simplified trace of the North Anatolian Fault Zone west of the of the Bolu basin, with its main three strands (NNAF, CNAF and SNAF) (see lower right inset for location of the area). Portions of the fault zone that ruptured during the 1999, earthquakes are shown. The mezoseismal areas (felt areas) of the historical earthquakes occurred near the Düzce fault segment are shown too (redrawn from Ambraseys and Finkel [1995]; Ambraseys [2002]; Atakan et al. [2002]; King et al. [2001]).

Because historical information is very limited, knowledge about recurrence of large earthquakes on the Düzce fault can be derived only from paleoseismology. Soon after the 1999 earthquakes several paleoseismological investigations were carried out at different locations along the fault (tab. 3.3.2). On the basis of trenching Hitchcock et al [2003] find evidence for three to

five paleoearthquakes in the past 2100 years, with a recurrence interval ranging from 300 to 800 years and the penultimate event occurred about 300 years ago. Komut [2005] recognized 6 paleoevents since BC1750 with the one prior to 1999 occurring during the past 500 years. Emre et al. [2001, 2003a and 2003b] found evidence for three paleoearthquakes since AD665, the oldest and the youngest of which are dated AD665-1050 and AD1650-1750, respectively. Finally, by paleoseismological geo-slicing and coring investigations, Sugai et al. [2001] developed a surface faulting history for the past 2 millennia at a site in the western part of the fault. Here, these authors recognize four possible/probable paleoearthquakes preceding 1999 and suggest an average recurrence time of 4-500 years.

Reference	**Paleoevents (N)**	**Recurrence interval (yrs)**	**Penultimate event (AD)**
Komut [2005]	3-5	300-800	1700
Hitchcock et al [2003]	6		>1500
Emre et al. [2001, 2003a and 2003b]	3	300-450	1700
Sugai et al. [2001]	4	400-500	

Table 3.3.2. Main results of the paleoseismological investigations performed along the Düzce fault.